JAERI-Research
99-062

THE JT-60U 2.45 MeV NEUTRON TIME-OF-FLIGHT SPECTROMETER

November 1999

Magnus HOEK, Takeo NISHITANI, Hiroyuki TAKAHASHI*,
Masaharu NAKAZAWA*, Thomas ELEVANT*
and Yasunari SHIBATA

日本原子力研究所
Japan Atomic Energy Research Institute

本レポートは、日本原子力研究所が不定期に公刊している研究報告書です。
入手の問合わせは、日本原子力研究所研究情報部研究情報課（〒319-1195　茨城県那珂郡東海村）あて、お申し越し下さい。なお、このほかに財団法人原子力弘済会資料センター（〒319-1195　茨城県那珂郡東海村日本原子力研究所内）で複写による実費領布を行っております。

This report is issued irregularly.
Inquiries about availability of the reports should be addressed to Research Information Division, Department of Intellectual Resources, Japan Atomic Energy Research Institute, Tokai-mura, Naka-gun, Ibaraki-ken 319-1195, Japan.

編集兼発行　日本原子力研究所

The JT-60U 2.45 MeV Neutron Time-of-Flight Spectrometer

Magnus HOEK, Takeo NISHITANI, Hiroyuki TAKAHASHI*, Masaharu NAKAZAWA*, Thomas ELEVANT** and Yasunari SHIBATA

Department of Fusion Plasma Research
Naka Fusion Research Establishment
Japan Atomic Energy Research Institute
Naka-machi, Naka-gun, Ibaraki-ken

(Received October 28, 1999)

A 2.45 MeV neutron time-of-flight spectrometer was designed and built for measurements of neutron energy spectra from the JT-60U Tokamak. The spectrometer consists of two fast plastic scintillators (50 cm^2 and 1800 cm^2, thickness: 2 cm) where each detector is located on two constant time-of-flight spheres. The time-of-flight spheres have radius of 1 m which gives a neutron flight length of ~164 cm and a time-of-flight of ~92 ns for 2.45 MeV source neutrons. The calculated spectrometer efficiency and resolution are 2.8×10^{-2} cm^2 and 105 keV (4.3%), respectively. The energy resolution corresponds to a time resolution of 2.0 ns. The spectrometer will measure neutrons in a vertical line-of-sight, ~9 m from the plasma center. For a total neutron emission of 10^{16} n/s, the countrate in the first scattering detector, located in the neutron beam, is estimated to ~2.5 MHz. The useful countrate for this case is estimated to ~6 kHz which gives a neutron energy spectrum sampling time of ~100 ms. This paper describes the principle of the spectrometer, a method for energy calibration of the scintillator detectors and timing tests of the big scintillator detector. We could also test the complete system utilizing 14 MeV neutrons where the results from the coincidence measurements confirmed the Gaussian shaped response functions, the efficiency and the resolution as calculated by Monte Carlo. A method for random background correction is proposed and line-of-sight effects and analysis of neutron spectra from Maxwellian and non-Maxwellian plasma are discussed.

Keywords: Fusion, Plasma, Diagnostic, Neutron, Time of Flight, Spectrometer, Ion Temperature, Response Function, Scintillator, Energy Calibration

---

* The University of Tokyo, Dept. of Quantum Engineering and Systems Science
7-3-1 Hongo, Bunkyo-ku, Tokyo 113-8656, Japan

** The Alfvén laboratory, Royal Institute of Technology, Stockholm, Sweden

JT-60U用2.45 MeV中性子飛行時間スペクトロメータ

日本原子力研究所那珂研究所炉心プラズマ研究部
Magnus HOEK・西谷　健夫・ 高橋　浩之*・中沢　正治*
Thomas ELEVANT**・柴田　泰成

（1999年10月28日受理）

JT-60Uにおける中性子エネルギースペクトルの測定を目的として、2.45 MeV中性子用の飛行時間スペクトロメータを設計・製作した。本スペクトロメータは2つの高速プラスチックシンチレータから成り、それぞれ2つの等飛行時間球面に沿うように配置した。等飛行時間球面の半径は1m、第1検出器～第2検出器間の距離は約1.64 mとした。したがって2.45 MeV中性子に対する散乱中性子の飛行時間は約92 nsとなる。計算により評価した検出効率とエネルギー分解能はそれぞれ、2.8×10^{-2} cm^2と105 keV (4.3%)となる。このエネルギー分解能は2 ns の時間分解能に対応している。JT-60Uにおいて、このスペクトロメータはプラズマ中心から約9m下に設置さる。10^6 n/sの全中性子発生率のとき、第1検出器の計数率は約2.5 MHz, 有効計数率約6 kHzと評価されるので、約100 ms毎にスペクトルを測定することが期待できる。本報告ではスペクトロメータの原理、プラスチックシンチレータ検出器のエネルギー較正方法及び大形第2検出器のタイミングテストについて紹介する。また14 MeV中性子を使用して、本スペクトロメータシステムの試験を行い、応答関数がガウス型であること、及び検出効率とエネルギー分解能がモンテカルロ計算と一致することを確認した。さらに、ランダムコインシデンス補正、視野の線積分効果、マックスウェル及び非マックスウェル速度分布プラズマの中性子スペクトルについて議論する。

那珂研究所：〒311-0193　茨城県那珂郡那珂町向山801-1
＊　東京大学
＊＊　王立工科大学アルフヴェン研究所

Contents

目　　次

This is a blank page.

1. Introduction

Neutron diagnostic of fusion plasmas comprises several means. The most common neutron diagnostic is the measurement of the total neutron emission, which is related to the number of fusion reactions occurring in the plasma. This can be achieved by either neutron activation of foils (time integrated) [1] or by fission chambers [2] with a sampling frequency of up to 1 kHz. Also, spatially resolved neutron emission measurements with a total of 19 line-of-sights with 1 liquid scintillator detector for each line-of-sight, is in use at JET [3]. These diagnostics measure the countrate above certain threshold- or discriminator levels. However, although the neutrons from a fusion plasma are commonly regarded as monoenergetic (2.45 MeV or 14.1 MeV depending on the reacting species of the fusion reactions), the energy spectrum of the neutrons is also of interest. The neutron energy distribution is affected by the movement of the reacting plasma ions and therefore depends on the ion temperature of the plasma. For ohmically heated plasmas, the ion velocity distribution is, in general, Maxwellian. In the case of heating by injection of neutral deuterons, Neutral Beam Injection (NBI), the deuteron velocity distribution becomes non-Maxwellian and the energy distribution changes accordingly.

For Maxwellian plasmas, it is possible to deduce an analytical expression for the neutron energy spectrum (see refs. [4] and [5]). Regardless if the plasma consists of deuterium only (DD-plasma), or is a mixture of deuterium and tritium (DT-plasma), the neutron energy spectrum has approximately a Gaussian shape according to:

$$f(E) \propto -\frac{(E - E_{mean})^2}{2\sigma^2} \qquad [1]$$

where E_{mean} is the average neutron energy and σ is the standard deviation.

The relation between the width of the neutron energy peak, ΔE_{FWHM}, and the ion temperature of the plasma, T_i, can be written as:

$$\Delta E_{FWHM} \approx k\sqrt{T_i} \qquad [2]$$

where ΔE_{FWHM} and T_i are in units of [keV] and $\Delta E_{FWHM} \approx 2.35\sigma$. The constant k is weakly dependent on both T_i and E_{mean} [6] and is ~82.6 for 2.45 MeV neutrons (DD-plasma) and ~177 for 14.1 MeV neutrons (DT-plasma).

From the above is then realized that, assuming a Maxwellian plasma, the ion temperature of the plasma can be calculated from the measurement of the width of the neutron energy distribution. For a deuterium plasma with an ion temperature of 4 keV, the width of the energy distribution becomes 165 keV (Eq. [2]) or 6.7 %. If neutron

spectrometry will be used for ion temperature measurements, the energy resolution should therefore be better than 6.7 %. The design of neutron t-o-f spectrometers with an energy resolution of a few percent is not easy, especially as high energy resolution and high efficiency (or short sampling times) contradict each other in terms.

In the case of a plasma heated by injection of neutral deuterium (NBI), there will be three different neutron sources, all with the same energy of the source neutrons, depending on which reaction process that occur. For NBI heated plasmas the neutrons are generated by either beam-beam (bb) ions, beam-plasma (bp) ions or plasma-plasma (pp) ions. In most cases the neutrons from bp-reactions dominate and the width of the neutron energy distribution is therefore determined by the (known) energy of the injected deuterium. However, analysis of neutron energy spectra can also give information regarding the fractions of bb- bp- and pp-neutrons [7]. A theoretical description [8] can be compared with the measured one, and a consistency check can be made. In the case of unknown parameters in the theoretical description, a best fit can be made with the measured distribution by varying the free parameters. From such a fit and for a NBI heated plasma (where deuterons are injected), it is then possible to e.g. determine the fractions bb-, bp- and pp-reactions that has occurred. Neutron spectrometry has therefore become a necessary tool in plasma diagnostics.

The most successful techniques for measurements of neutron energy distributions from fusion plasmas are ^{3}He-spectrometers [9] and neutron time-of-flight (t-o-f) spectrometers [7] [10] [11]. The energy resolution of the ^{3}He-spectrometer is very good (~40 KeV) but the sampling time is as long as a few seconds. Furthermore, the response functions are complicated, which means that an unfolding procedure is difficult. The energy resolution for the t-o-f-spectrometers used so far is ~120 keV with sampling times of ~100 ms (assuming the neutron yield is high enough). The response functions are Gaussian in most cases. Neutron t-o-f-spectrometers for 14.1 MeV neutrons have also been designed and built [12] where one is in use at the JET Tokamak.

A 2.45 MeV neutron spectrometer has been proposed for the JT-60U Tokamak [13] [14]. The design, construction and tests, utilizing γ-sources, of this spectrometer were done in collaboration with the University of Tokyo, Dept. of Quantum Engineering and Systems Science and the results will be described in this paper. We could also test the spectrometer utilizing 14 MeV source neutrons at the FNS [15] facilities in JAERI Tokai and the results from these measurements will be shown.

2. Description of the spectrometer

The neutron spectrometer is based on the principle of measurement of the t-o-f between two fast (~ns) plastic scintillators (see fig. 1). The source neutrons, which enter through a collimator, interact with the first scintillator (D0) located in the neutron beam. The amplitude of the generated signal is dependent on the scattering angle of the neutron,

which implies that an energy discriminator window can be utilized. Some of the scattered neutrons are detected by a second large scintillator (D1) and a second coincidental time signal is generated. The t-o-f of the neutron is the time difference between the two signals.

For monoenergetic source neutrons, the energy of the scattered neutrons depends on the scattering angle. To keep the time resolution as good as possible, the detectors are positioned on a "constant t-o-f sphere". It can be shown that for neutrons that scatter in the lower pole of the sphere (in the central point of the D0-detector), the t-o-f to another point on the spherical shell is independent of the scattering angle. Therefore, to achieve a constant t-o-f for mono-energetic source neutrons and to accomplish a high efficiency, a big D1-detector has been chosen (30x60 cm^2, 2 cm thickness). The detector is also bent in such a way that it follows the constant t-o-f sphere. The major limiting factor of the scintillator size is the attenuation and timing deterioration of the generated light during its way to the photo-cathode of the PM-tube. Therefore, two PM-tubes are connected via adiabatic light guides to the 30x2 cm^2 edges of the D1 scintillator and the distance between the scintillator edges has been limited to 60 cm. The time signals from these two photo-multiplier (PM) tubes are then averaged, utilizing a mean-timer module, to minimize the deterioration of the D1 time signal.

The concept of a constant t-o-f sphere has been taken one step further by introducing a second constant t-o-f sphere. For this sphere, the D0-detector approximately follows the spherical shell while the central point of the D1-detector is positioned on the sphere. The D0-detector is tilted -70° to reduce the time spread.

2.1 Electronic setup

The electronic setup consists of mainly three branches (see fig. 2). Two branches are used for the timing (start and stop) and the third branch is used to create a gate for the start signal. For the planned position at the JT-60U Tokamak (see fig. 3), typical expected count rates of the D0-detector are in the MHz range (see table 1). The average dead time of the Time-to-Amplitude converter (TAC) is ~1 μs per accepted start, which is unacceptable for a start rate in the MHz range. Therefore, delaying the signal from the D0-detector so it comes after the signal from the D1-detector reverses the start-stop sequence between the detectors and reduces the start rate considerably.

For an event in the D1 scintillator, the generated light is transferred via the light guides to the photo cathodes of the PM-tubes. The bases (voltage dividers) attached to the PM-tubes are passive bases and to avoid voltage-drifts during high count rates, we have decided to keep a low level (1000-1200 V) of the HV applied to the PM-tubes. However, at these low HVs, the output signals need to be amplified by pre-amplifiers. The time signal is then fed into constant fraction discriminators (CFD) and if the amplitude exceeds the discriminator level, a fast NIM signal is generated. These NIM signals are

fed into a mean-timer module, which averages the time signals from the large D1 scintillator. This averaged D1 time signal is used as a START signal for the time-of-flight measurement.

The gate for the start signal is accomplished by connecting the dynode outputs from the two D1 PM-tubes (D1.1 and D1.2), via pre-amplifiers and fast filter amplifiers, to a "Sum and Inverter" module. The summed D1 signal is fed to a Constant Fraction Differential Discriminator (CFDD) which supplies the gate signal to the gate input of the TAC. The Sum and Inverter module is slow, which means that the D1 timing signal needs to be delayed ~250 ns to coincide with the gate signal. Furthermore, due to the reversed start-stop sequence, the timing signal from the D0-detector needs to be delayed by the same amount in addition to the delay required for the reversed start-stop sequence.

To minimize background event rates, a CFDD is employed for the D0-detector as well. A pulse amplitude window is set which has been calibrated to correspond to the interesting energy range of the recoil protons in the D0-detector. If the amplitude of the signal falls within the selected window, the CFDD module provide a fast output NIM signal to the STOP channel of the TAC.

2.2 Calibration of the detectors

By our selection of electronics, we can define a discriminator window for both the D0 and the D1-detector. The widths of the windows are set by the CFDDs where the CFDD in the D1-detector branch controls the gate. To relate the signal amplitude to the energy of the recoil proton (from neutron scattering with hydrogen), we need to do a calibration. For the energy calibration of the scintillators, we use the same method that were described in refs. [16] and [17].

For the calibration, we use γ calibration sources. γs scatter in plastic material by mainly Compton scattering, which means that the light signal arises from electrons slowing down in the scintillator. However, the amplitude of a signal generated by e.g. 1 MeV γs is not the same as the amplitude from a 1 MeV recoil proton. Therefore, we need to know the relation between the energy of the protons and electrons that give rise to the same amplitude of light. We have used a modified version of Madey's relation ([18], [19]) which is valid for the proton energy range 0.34 – 14.5 MeV for the NE102 plastic scintillator:

$$E_{e^-} = A_0 + A_1\left[1 - \exp(-A_2 \cdot E_p^{A_3})\right] + A_4 \cdot E_p \qquad [3]$$

where E_{e^-} is the electron energy [MeV] and E_p is the proton energy [MeV]. The coefficients are as follows: $A_0 = 0.05957$, $A_1 = -1.2741$, $A_2 = 0.5096$, $A_3 = 1.1422$ and $A_4 = 0.6120$.

For the geometric setup of the spectrometer, according to fig. 1, and for the coincidence criterion to hold, the neutrons scatter in the interval [30° - 40°] in the D0-detector. The source neutron energy interval of interest is [1.6 MeV – 3.6 MeV] which gives a recoil proton energy interval of [0.4 MeV – 1.5 MeV]. For the same light output in the scintillator (see Eq. 3), this corresponds to an electron energy interval of [100 keV – 270 keV].

The interesting energy interval of the neutrons that enter the D1-detector is [0.9 MeV – 2.7 MeV]. This means that the maximum recoil proton energy is 2.7 MeV, which corresponds to an electron energy of 700 keV.

Fig. 4 shows the relation between the proton energy and the corresponding electron energy for the same light output according to Eq. 3. The relevant energy intervals for both detectors are also indicated.

Table 2 lists some standard γ-calibration sources. The γ-energies of the sources are transformed to the corresponding Compton edge energies, E_c, that is registered by a scintillator. From the table, one realize that ^{51}Cr would be a suitable source for the calibration of the D0-detector while ^{88}Y would be appropriate for the calibration of the D1-detector. However, in this work, the only source we had access to was ^{22}Na with a Compton edge energy of 341 keV. The calibrations were therefore done with this source only. The Compton edge energy of ^{22}Na is also indicated in fig. 4 as a reference.

The principle of the calibration is to scan the applied HV of the PM-tubes and count the pulses that exceed a fixed discriminator level.

If the amplitude of the signal from a PM, A, with an applied HV, V, is proportional to the light signal from a particle depositing an energy E in the scintillator, εE, we can write the signal level as:

$$A = \varepsilon \cdot E \cdot k \cdot V^n \quad [4]$$

where n is a constant proportional to the number of dynodes of the PM-tube.

If the calibration energy is E_0 we can rewrite Eq. 4 as:

$$\ln(A_i) = K_{0i} + n_i \cdot \ln(V) \quad [5]$$

where

$$K_{0i} = \ln(\varepsilon_i \cdot E_0 \cdot k_i) \quad [6]$$

The constants K_{0i} and n_i we define as the "calibration parameters" for detector i. If the signal differential countrate is plotted as a function of the applied HV, a peak will appear. This peak corresponds to at which HV the Compton edge energy at E_0 (electron energy) exceeds the fixed discriminator level. By plotting the level of the discriminator versus the peak position [HV] in a log-log plot (cf. eq. 5), a straight line will occur. The slope and intercept of this line become our calibration parameters.

When the set of calibration parameters $\{K_{0i}, n_i\}$ are known, it is now possible to find such voltages, V_i, that the amplitude of the signals are the same for the same γ-energy but for different detectors. However, we also need to know the relation between the electron energy and the amplitude of the signal.

The calibration parameters were obtained for a certain used γ-energy, E_0. If we rewrite Eq. 4 as:

$$A_i(E,V) = \frac{E}{E_0} C_{0i} V^{n_i} \quad [7]$$

where

$$C_{0i} = \varepsilon_i \cdot E_0 \cdot k_i \quad [8]$$

then we can calculate the amplitude of the signal depending on the γ-energy, E, and the calibration parameters $\{K_{0i}, n_i\}$ for detector i. Note that E and E_0 refers to the electron energy. In the case of proton energy, one need to convert from proton energy to electron energy, utilizing Eq. 3, before insertion in Eqs. 7 and 8.

In fig. 5 the discriminator level is plotted versus the peak positions [HV] of the differential countrate for the three detectors, D0, D1.1 and D1.2. From the figure, it is realized that the slopes are roughly equal which indicates that the number of dynodes for

each PM-tube is the same. (The tubes were the same model and came from the same manufacturer). We can also see that although the D1.1 and D1.2-detectors are identical with the same interface between the photo cathode and the scintillator, the D1.2-detector is more sensitive than the D1.1-detector. Apart from unavoidable differences between the PM-tubes themselves, the optical connection between the scintillator and the detector can never be made identical which gives the difference in sensitivity. Table 3 lists the measured calibration parameters for that particular measurement. However, it should be emphasized that for the final setup of the spectrometer and electronics, the calibration procedure needs to be redone while the K_0 calibration parameter is strongly dependent on the cable lengths.

To check the validity of the calibration, we set an applied HV on the D0-detector and calculate the signal levels [mV] for the γ-lines of the source. Na-22 emits two γ-lines, 511 keV and 1274 keV, which corresponds to the Compton edge energies 341 keV and 1062 keV, respectively. Using the calibration parameters in table 3, we can then calculate the signal levels according to:

$$A_{341keV}(E,V) = \frac{E}{E_0} C_0 V^n = \frac{341}{341} e^{-100.155} \cdot 1200^{15.1522} = 1444\,mV$$
$$A_{1062keV}(E,V) = \frac{E}{E_0} C_0 V^n = \frac{1062}{341} e^{-100.155} \cdot 1200^{15.1522} = 4497\,mV \qquad [9]$$

Fig. 6 shows the amplitude distribution for a measurement where the lower and upper discriminator levels are set to the values calculated by Eq. 9. Also shown is the spectrum with a maximum amplitude window (LLD: 100 mV, ULD: 5 V). It is clear that the discriminator levels indeed cut the signal amplitude at approximately half the height of the Compton edge for each of the two Compton edge energies.

2.3 Timing measurements

Perhaps the most critical part of the spectrometer is the time resolution of the big D1 scintillator. The length of the scintillator is 60 cm, which corresponds to a photon flight time of 3.2 ns (refractive index: 1.58). The measured time differences of the two D1-detectors are shown in fig. 7 and fig. 8 where a Na-22 source was positioned on the 30x60 cm^2 surface at 6 and 9 different positions, respectively.

Fig. 7 shows the average pulse shape (from 1000 events) from the anode outputs of D1.1 (solid line) and D1.2 (hatched line). The measurement was achieved by digitizing the output pulses of both detectors into 2x512 channels per event, with a channel width of 0.2 ns. The time difference between the two pulses was calculated by correlation using the fast Fourier transform [20]. When the source is positioned in the middle of the detector (3 plots at the left side), the pulses appear approximately simultaneously. For

source positions close to the D1.2-detector (right detector position, 3 plots at the right side) the D1.2 signal appear ~3-3.4 ns before the D1.1 signal as expected.

In the left plots of the figure (middle source position), it looks like as if the pulse corresponding to the D1.2 signal has a slower rise-time than the D1.1 signal. The reason for this is that in the digitizer measurement, an event is triggered by the occurrence of a D1.1 signal where the single trigger starts the data collection for both channels. If we would have access to a digitizer with independent triggers, the pulses would most likely have the same shape. This effect also affects the calculation of the time positions. When the correlated times for each event are plotted in a histogram, the data for source positions close to the D1.2 detector form a Gaussian while this is not the case for positions in the vertical middle of the scintillator. This effect can explain why the measurements for the middle source position give an offset of the timing signals.

Fig. 8 shows the result from a measurement where the anode pulses (via CFDs) are fed to the start- and stop-inputs, respectively, of a TAC. For this measurement, the D1.1 signal was delayed by ~50 ns. The three plots in the figure corresponds to the three vertical source positions while the three curves in each plot correspond to the horizontal source positions on the scintillator. Here, the time spectra, corresponding to the difference between the timing signals, are positioned symmetrically around the vertical center source position at ~±4 ns. It is surprising that the number of counts under each spectrum is different with different vertical positions of the source. One could expect that the number of registered counts would be highest for the middle source positions on the D1 scintillator. In our case, the number of counts decreases with the vertical source position. The reason for this is not clear.

The timing uncertainty introduced by the large scintillator is unacceptable and therefore a mean-timer module is used to average the time of arrivals of the D1-detector pulses. As will be shown later (see fig. 11), the total time resolution of the whole system, with 14.1 MeV neutrons and with the mean-timer installed, was obtained as 1.1 ns.

2.4 Coincidence measurements

For a check of the electronics and the following data sampling and analysis, we tested the spectrometer utilizing the Fusion Neutronics Source (FNS) neutron generator [15]. Unfortunately, at that occasion we only had access to 14.1 MeV neutrons and a small collimator (1 cm radius) between the DT-target and the D0-detector. The small collimator made it impossible to check the improvement of the resolution with the tilt angle of the D0-detector. Nevertheless, both the measured efficiency and the resolution of the spectrometer were confirmed by Monte Carlo calculations [14].

The tilted D0-detector was positioned ~5 m from the DT target at an angle of 80° from the ion-beam and the 14.1 MeV neutrons were collimated by a long collimator with ~1 cm radius (see fig. 9). The energy windows of both the D0- and the D1-detectors were set at maximal width. In our measurements, we could register a "γ-flash" from the target, which gave us a time reference for our time-scale of the time distribution. The distance between the coincidence peak from the neutrons and from the flash target γ was ~33 ns. Theoretically, the flight time for neutrons and γ is ~38.5 ns and ~5.5 ns, respectively, which gives a difference in flight time of ~33 ns.

For these measurements, we could not make a calibration of the signal levels. The cable lengths were much longer than at our earlier calibrations and the access to the experiment hall was limited. Therefore, only a simple check of the discriminator- and signal levels of the D0-detector was done as follows;

The maximum anode signal from the D0-detector was ~3V. The proton energy range from scattering of 14.1 MeV source neutrons is [$0 < E_p < 14$ MeV] which corresponds to the electron energy range [$0 < E_{e^-} < 7.35$ MeV] (cf. Eq. 3). This gives us a scaling of the electron energy per V as 2450 keV/V. For coincidences to occur, the proton energy range is [3.5 MeV $< E_p < 5.8$ MeV] which corresponds to [1080 keV $< E_{e^-} < 2360$ keV]. This means that the signals, which give rise to coincidences, should be in the range [440 mV $< A < 1000$ mV]. Fig. 10 shows the neutron coincidence time spectra with the LLD of the D0 detector as a parameter. From the figure it is evident that the neutron peak diminishes at ~1000 mV while it is unchanged in the discriminator range [100 mV $< A < 400$ mV] and this confirms our calculations.

Fig. 11 shows the measured time-of-flight spectrum with the derived energy spectrum, compared with the spectrum calculated by the Monte Carlo code McTOF [14]. For the Monte Carlo calculations, the sampled interaction area of the D0-detector was set to be the same as the area dimensions of the collimator. The measured time resolution for the whole system was obtained as 1.1 ns in agreement with the Monte Carlo calculations (1.2 ns).

The energy distribution was calculated from the measured time distribution. For the calculations we have to assume certain neutron interaction fix points in the detectors. These points were set at the center of each detector. The selection of these interaction coordinates gives a neutron scattering angle of 35° (in the D0 detector) and a flight distance of 163.8 cm between the detectors. The position of the γ-peak in the time distribution was set as 5.5 ns.

The resolution of the derived energy distribution was obtained as 830 keV. The neutron source itself has a width of 145 keV, which gives 820 keV energy resolution (or 5.8 %) for the spectrometer. The resolution obtained from the Monte Carlo calculation

was 6 % higher (870 keV). For 2.45 MeV neutrons, the resolution is expected to improve due to the longer flight time of the scattered neutrons between the detectors.

We could also confirm the efficiency of the spectrometer as calculated by Monte Carlo (2.7×10^{-4}). From the number of monitored target neutrons and the distance between the target and the D0-detector, we could estimate the number of neutrons that would hit the D0-detector. A Gaussian fit to the energy distribution was made where the fraction $Area_{Gauss}$/D0-hits gave the efficiency. The measured efficiency was 3.1×10^{-4}, which is 15 % higher than the calculated efficiency.

2.5 Random coincidence correction

In the measured time spectrum shown in fig. 11, a background appears throughout the spectrum. This background comes from random coincidences where the TAC measurement is stopped by an uncorrelated event in the stop detector.

For low count rates, the random coincidence rate is determined by [21]:

$$\frac{dB(n)}{dt} = r_1 r_2 \Delta\tau \qquad [10]$$

where B(n) is the random coincidence background in spectrum channel n, r_i is the count rate of detector i and $\Delta\tau$ is the spectrum channel width.

The random coincidence background is obtained by integration over the spectrum data-taking interval ΔT:

$$B(n) = \int_{\Delta T} r_1 r_2 \Delta\tau \; dt \qquad [11]$$

Therefore, to achieve random correction we need to count the signals that are input to the TAC. In our prototype spectrometer, we did not have access to scalers and this correction was therefore not tried.

For high count rates, further effects such as "time shielding" and dead time effects should be corrected for [7].

2.6 Estimated sampling time for a neutron spectrum

For any type of spectrometer that aims to measure the neutron energy distribution of fusion plasmas, it is desirable to know what energy resolution the spectrometer should posses and how many events that are necessary for a "good" spectrum. Generally, if we

want to resolve a spectrum with a certain width, our neutron spectrometer should at least have the same resolution as the width of the measured spectrum.

Assume that the neutron spectrum from the plasma and the response function of the spectrometer are Gaussian. We then have the following relation between the desired relative error of the ion temperature of the plasma, dT_i / T_i, and the necessary number of counts, N, in a measured neutron spectrum [22]:

$$\frac{dT_i}{T_i} = \sqrt{\frac{2}{N}}\left(1 + \frac{R^2}{W^2}\right) \qquad [12]$$

where R is the resolution of the spectrometer, and W is the width of the neutron spectrum. Plasmas near thermal equilibrium, e.g. ohmically heated Tokamak plasmas, have in general Maxwellian ion velocity distributions. For Maxwellian plasmas, the width, W (FWHM), of the neutron energy distribution is therefore proportional to $\sqrt{T_i}$ where T_i is the plasma ion temperature. W can be expressed as:

$$W = 82.6\sqrt{T_i} \qquad [13]$$

which is valid for a Maxwellian DD-plasma with a Gaussian neutron energy distribution.

Fig. 12 shows the relative error of the measured ion-temperature versus the number of necessary counts, with the ion-temperature as a parameter. In the plot, an energy resolution of 105 keV of the spectrometer is assumed. If we want to measure an ion temperature of e.g. ~2 keV with 10 % resolution, we need ~700 counts in the measured spectrum. If we assume a total neutron yield from the plasma of 5×10^{14} n/s, the useful count-rate of the spectrometer is ~300 cps which means that 2-3 s measurement time is necessary (see ref. [13] and table. 1). However, for a neutron yield of 10^{16} n/s the useful count-rate is estimated to 6000 cps which means that 5-10 spectra might be recorded per plasma pulse. Fig. 13 shows the ion temperature as a function of the total neutron emission for two operation regimes of JT-60U, the Reversed shear and the High β-poloidal regimes. Initially it is expected that the spectrometer will measure the ion temperatures in the Reversed shear regime where it is estimated that 80% of the neutrons are Maxwellian and the rest come from beam-plasma fusion reactions.

2.7 Line-of-sight effects

The spectrometer will be located below the Tokamak and will measure the emitted neutrons in a vertical line-of-sight (see fig. 3). This means that the measured neutron energy distribution will be line-integrated. The measurement is further complicated by the fact that the plasma is inhomogeneous along the line-of-sight. Still, for most Tokamak plasmas, the neutron emission profile is strongly peaked in the center. This is due to the

deuterium density, to which the neutron emission is directly proportional, scales as the electron density, which is highest in the central plasma.

The vertical line-of-sight is nearly perpendicular to the toroidal field, which means that the energy broadening of the neutrons mainly comes from ion motion perpendicular to the field. If the spectrometer would measure the neutrons along a horizontal line-of-sight, the energy broadening would come from ion motion along the field. For a Maxwellian plasma, this has no importance due to the isotropic emission of neutrons. However, a derived value of the ion temperature still needs to be increased by typically ~10 % [23].

For non-Maxwellian plasmas, the energy broadening will depend on the line-of-sight. RF-heating (tuned to the cyclotron frequency of deuterium) will increase the ion velocity perpendicular to the magnetic field and the consequential change of the neutron spectrum will therefore be registered by a vertical line-of-sight. For injected neutrals (NBI heating), the ionization mainly occur by electron collisions which gives a small pitch angle scattering. Injection of deuterium will affect the neutron energy distribution and the effects for different line-of-sights depend on the injection angle to the main toroidal field.

3. Conclusions

A 2.45 MeV plastic scintillator type neutron time-of-flight spectrometer for the JT-60U Tokamak has been designed, constructed and tested at the University of Tokyo. The instrument consists of two fast detectors, located on two constant time-of-flight spheres. To improve the efficiency, the 2nd scintillator (D1) was made as big as practically possible (30x60 cm^2, 2 cm thick) with 1 PM-tube connected to each 2x30 cm^2 edge. The time spread between the PM-tubes (D1.1 and D1.2) was measured as ~4 ns but this could be reduced by averaging the pulse of arrivals. Due to the expected high count rates of the 1st small (5x10 cm^2, 2 cm thick) neutron scattering scintillator (D0), the start-stop sequence was reversed by delaying the time signal by ~150 ns. The sum of the linear signals (dynode outputs) from the D1.1 and D1.2 detectors was used as a gate for the start signal from the D1 detector.

A method for energy calibration utilizing γ-sources was proposed. When the calibration parameters are obtained, a relation between the applied HVs, the discriminator levels [mV] and the recoil proton energy can be calculated.

For measurements of the plasma ion temperature, the necessary number of counts of a neutron spectrum depends on the resolution of the instrument and the ion temperature itself. For an ion temperature of ~3 keV and a spectrometer resolution of 105 keV (4.3 %), a spectrum of ~600 counts is necessary. With an instrumental efficiency of

$2.8x10^{-2}$ cm^2, the useful countrate is ~6000 cps, which gives a spectrometer sampling time of ~100 ms.

A prototype of the spectrometer was tested at the FNS neutron generator with 14.1 MeV source neutrons. The Gaussian shaped response functions, the resolution and the efficiency as calculated by Monte Carlo was confirmed.

Acknowledgements

One of us (M. Hoek) would like to express his gratitude for the granted EU-STF fellowship that made it possible to work for a period of 1.5 years at the University of Tokyo.

For the measurements at FNS (Fusion Neutronics Source) we are very grateful for Dr. Takeuchi's and Dr. Kaneko's efforts with the set-up of the measurement and the supervision.

References

[1] Report: M. Hoek, H-S Bosch and W. Ullrich, "Triton Burnup Measurements at ASDEX Upgrade by Neutron Foil Activation", Max-Planck Institut für Plasmaphysik, IPP I/320, Mar. 1999.

[2] T. Nishitani, H. Takeuchi, T. Kondoh, T. Itoh, M. Kuriyama, Y. Ikeda, T. Iguchi, and Cris W. Barnes, Rev. Sci. Instrum. 63 (1992) 5270

[3] F.B. Marcus et. al, Plasma Physics and Controlled Fusion, 33 (4) (1991) 277

[4] W.R. Faust and E.G. Harris, Nuclear Fusion 1 (1960)

[5] H. Brysk, Plasma Physics 15 (1973), and references therein.

[6] P. van Belle and G. Sadler, Basic and Advanced Diagnostic Techniques for Fusion Plasmas (Proc. Course and Workshop, Varenna 1986) Vol. III, EUR 10797 EN, CEC (1987) 767, and references therein.

[7] T. Elevant, D. Aronsson, P. van Belle, G. Grosshoeg, M. Hoek, M. Olsson and G. Sadler, Nucl. Inst. Meth. A306 (1991) 331

[8] J.G. Cordey, W.G.F. Core and J. Sheffield, Nucl. Fusion 15 (1975) 755

[9] S. Skalev and J.M. Cuttler, Nucl. Sci. Eng. 51 (1973) 52

[10] M. Olsson, "Fusion Plasma Diagnostics by Means of Neutron Spectrometry", Thesis, Paper II, Royal Institute of Technology, Alfvén Laboratory, Stockholm 1992, ISRN KTH/ALF/DA – 92/2 - SE

[11] M. Olsson, P van Belle, S Conroy, T Elevant and G. Sadler, Plasma Physics and Controlled Fusion, 35 (1993) 179

[12] G. Grosshoeg, D. Aronsson, K-H. Beimer, R. Rydz and N.G. Sjöstrand, Nucl. Inst. Meth. A249 (1986) 468

[13] T. Elevant, M. Hoek and T. Nishitani, "Design study of a time-of-flight neutron spectrometer for JT-60U", Japan Atomic Energy Research Institute Report JAERI-M 93-123 (1993)

[14] M. Hoek, T. Nishitani, H. Takahashi, M. Nakazawa and T. Elevant, "Results from Monte Carlo simulations of the neutron transport for the new 2.45 MeV neutron time-of-flight spectrometer for the JT-60U Tokamak", Submitted to Fusion Engineering and Design, March 1999.

[15] T. Nakamura, H. Maekawa, Y. Ikeda, and Y. Oyama, "A DT Neutron Source for Fusion Neutronics Experiments at the JAERI", Proc. Int. Ion Engineering Congress, Kyoto, Japan, September 12-16, 1983, p. 567, Institute of Electrical Engineers of Japan (1983).

[16] K. Drozdowicz, M. Hoek and D. Aronsson, Nucl. Inst. And Meth. A306 (1991) 315-330

[17] M. Hoek, K. Drozdowicz and D Aronsson, "Method of Energy Calibration of the TANSY Neutron Detectors", Report: CTH-RF-68, Chalmers University of Technology, Göteborg (1990)

[18] R. Madey, F.M. Waterman, A.R. Baldwin, J.N. Knudson, J.D. Carlson and J. Rapaport, Nucl. Inst. And Meth. 151 (1978) 445-450

[19] S. Croft and J.M. Adams, Harwell Laboratory Oxfordshire, England, Private communication

[20] W.H. Press, B.P. Flannery, S.A. Teukolsky and W.T. Vetterling, "Numerical Recipes. The Art of Scientific Computing", page 415, Cambridge University Press, ISBN 0-521-30811-9

[21] G.F. Knoll, "Radiation Detection and Measurements" (Wiley, 1979)

[22] O. N. Jarvis , "Neutron Detection Techniques for Plasma Diagnostics", pp. 353-379, "Diagnostics for Fusion Reactor Conditions" Varenna Workshop (1982), EUR 8351-I EN

[23] G. Sadler et. al, Europhysics Conference Abstracts, Vol. 10C, part I, pp. 105-108

Table 1. Spectrometer count-rates and integration times. Here the efficiency of the spectrometer is taken as $A_{D0}x4x10^{-4}$ cm^2 and a resolution of 110 keV (FWHM) is assumed. The conversion factor between total neutron emission and flux at D0 is set to $2.5x10^{-11}$.

n-yield [n/s]	n-flux [n/cm^2·s]	A_{D0} [cm^2]	D0 count rate [cps]	Useful countrate [cps]	Δt per spectrum [s]
$5x10^{14}$	$1.3x10^4$	50	$1.3x10^5$	300	2.0
$1x10^{15}$	$2.5x10^4$	50	$2.5x10^5$	600	1.0
$5x10^{15}$	$1.3x10^5$	50	$1.3x10^6$	3000	0.2
$1x10^{16}$	$2.5x10^5$	50	$2.5x10^6$	6000	0.1
$5x10^{16}$	$1.3x10^6$	5	$1.3x10^6$	3000	0.2

Table 2. Typical γ-calibration sources with the γ-energies, Compton edge energies, abundance and half-life. For the calibration of the detectors, the Na-22 source was used.

Source	E_γ [keV]	E_c [keV]	Abundance [%]	Half-life
Am-241	59.54	11	35.9	432.7y
Co-57	122.06	39	85.68	271.8d
Co-57	136.47	48	10.67	271.8d
Cr-51	320.08	178	9.85	27.7d
Na-22	511	341	90.57	2.6y
Sr-85	514.01	343	99.29	64.8d
Cs-137	661.66	477	84.70	30.2y
Mn-54	834.84	639	99.98	312.2d
Y-88	898.04	699	93.7	106.6d
Co-60	1253a	1041	99.9	5.3y
Na-22	1274.54	1062	99.93	2.6y
Y-88	1836.06	1612	99.37	106.6d

Table 3. Calibration parameters from a calibration done at the University of Tokyo. The K_0 parameter strongly depends on the cable lengths, which makes an in situ calibration necessary.

Detector	K_0	n	E_0 [keV]
$D0_{Anode}$	-100.155	15.1522	341
$D1.1_{Anode}$	-88.001	13.0602	341
$D1.2_{Anode}$	-90.796	13.4884	341

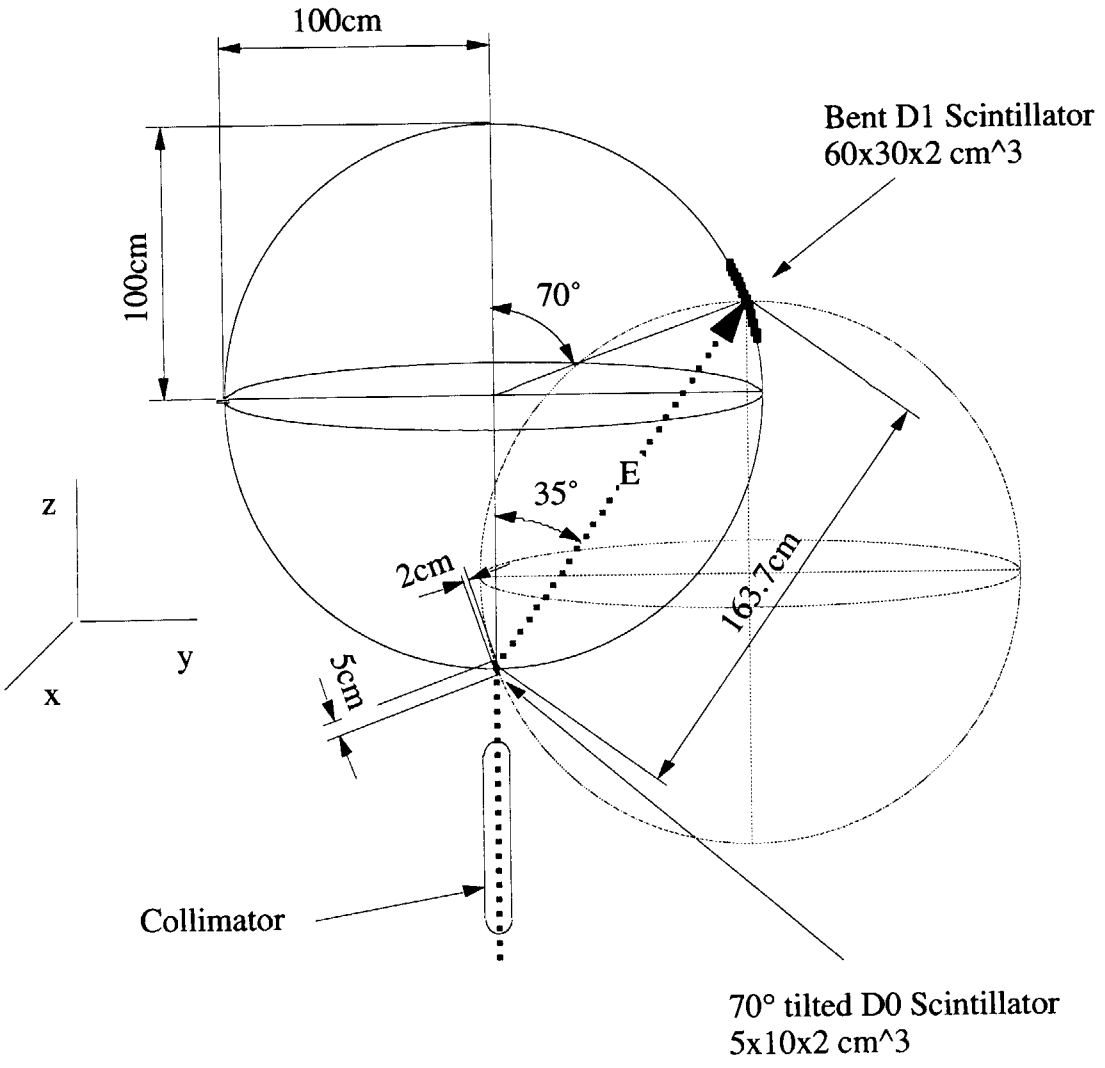

Figure 1. Principle of the JT-60U spectrometer. The resolution is optimized by the introduction of two time-of-flight spheres which is achieved by a 70° tilted D0 detector. The radii of the time-of-flight spheres are 100 cm and the neutron flight path between the detectors is 163.7 cm.

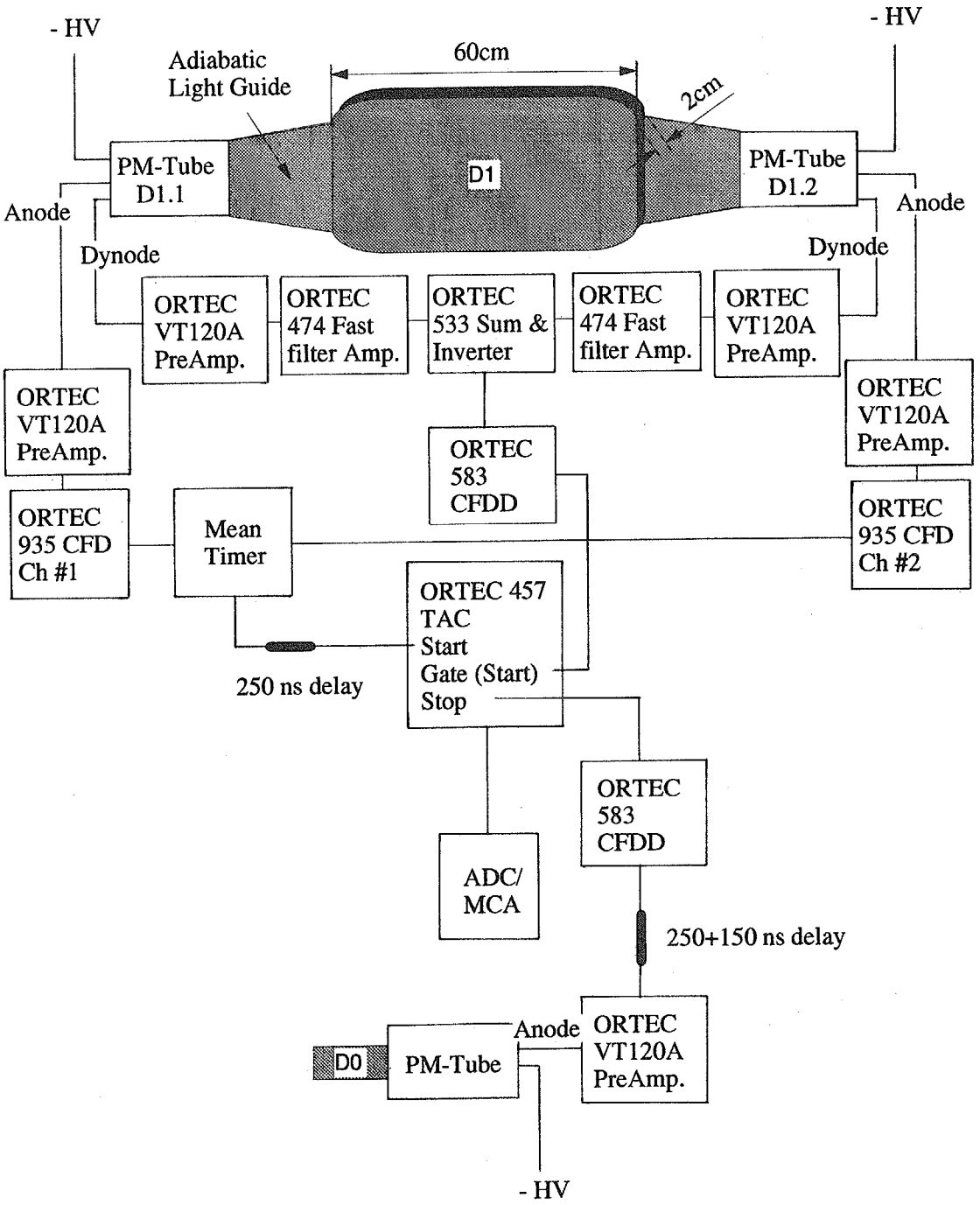

Figure 2. Electronic setup of the instrument. An event in the D1 detector gives a pulse in both the D1.1 and the D1.2 detectors. Fast logic pulses are generated by the CFDs and these signals are time-averaged in the MT-module. The output from the MT starts the clock of the TAC. If the sum of the amplitudes from the D1.1 and the D1.2 detector lies within the CFDD amplitude window, the gate for the start signal is open. For an event in the D0 detector, a fast logic pulse is generated by the CFDD and is used as a stop signal for the TAC.

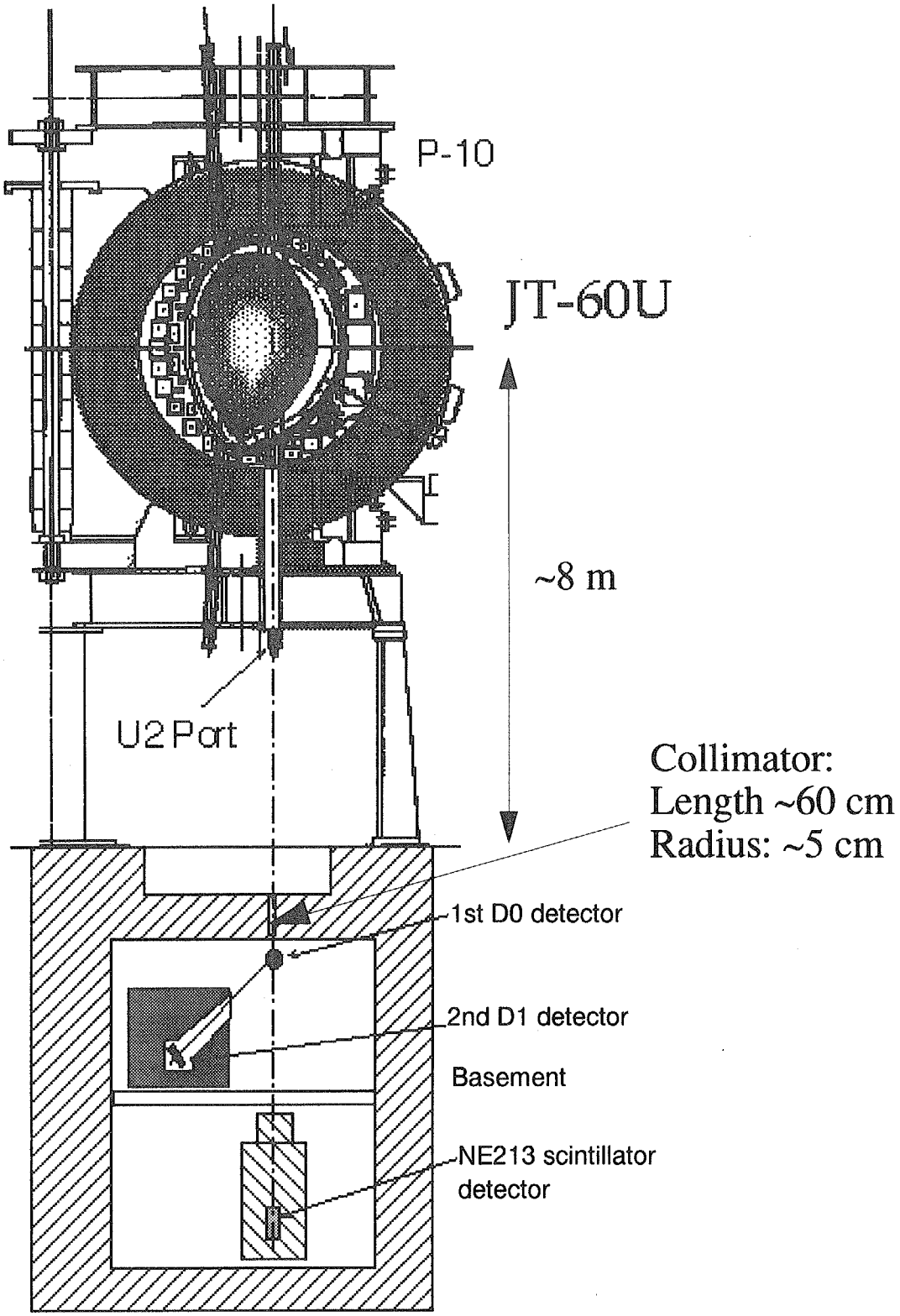

Figure 3. Arrangement of the 2.45 MeV neutron time-of-flight spectrometer at the JT-60U tokamak. An NE-213 scintillator neutron counter is also shown.

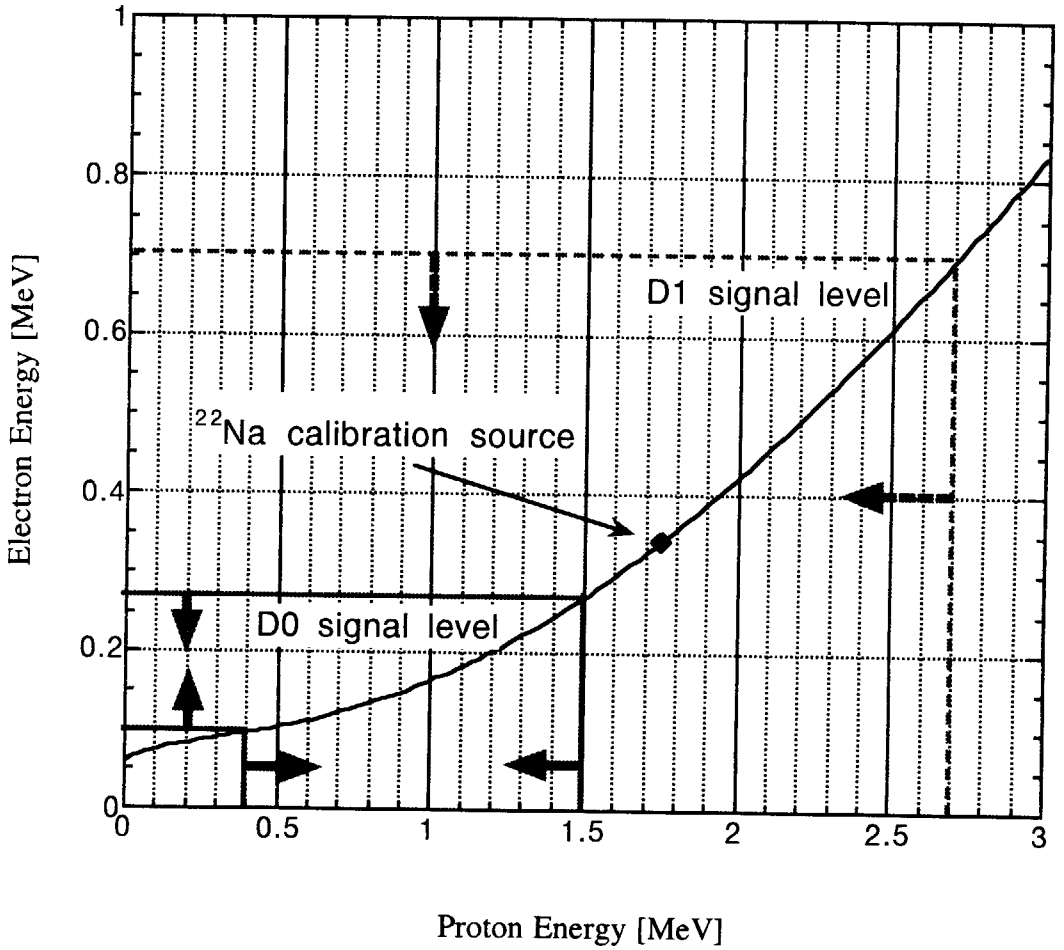

Figure 4. Relation between the proton energy and the corresponding electron energy for the same light output for a plastic scintillator (NE102). For our calibration, we have utilized a Na-22 with a Compton edge energy of 341 keV. The relevant signal levels for both the D0- and the D1-detector are also indicated.

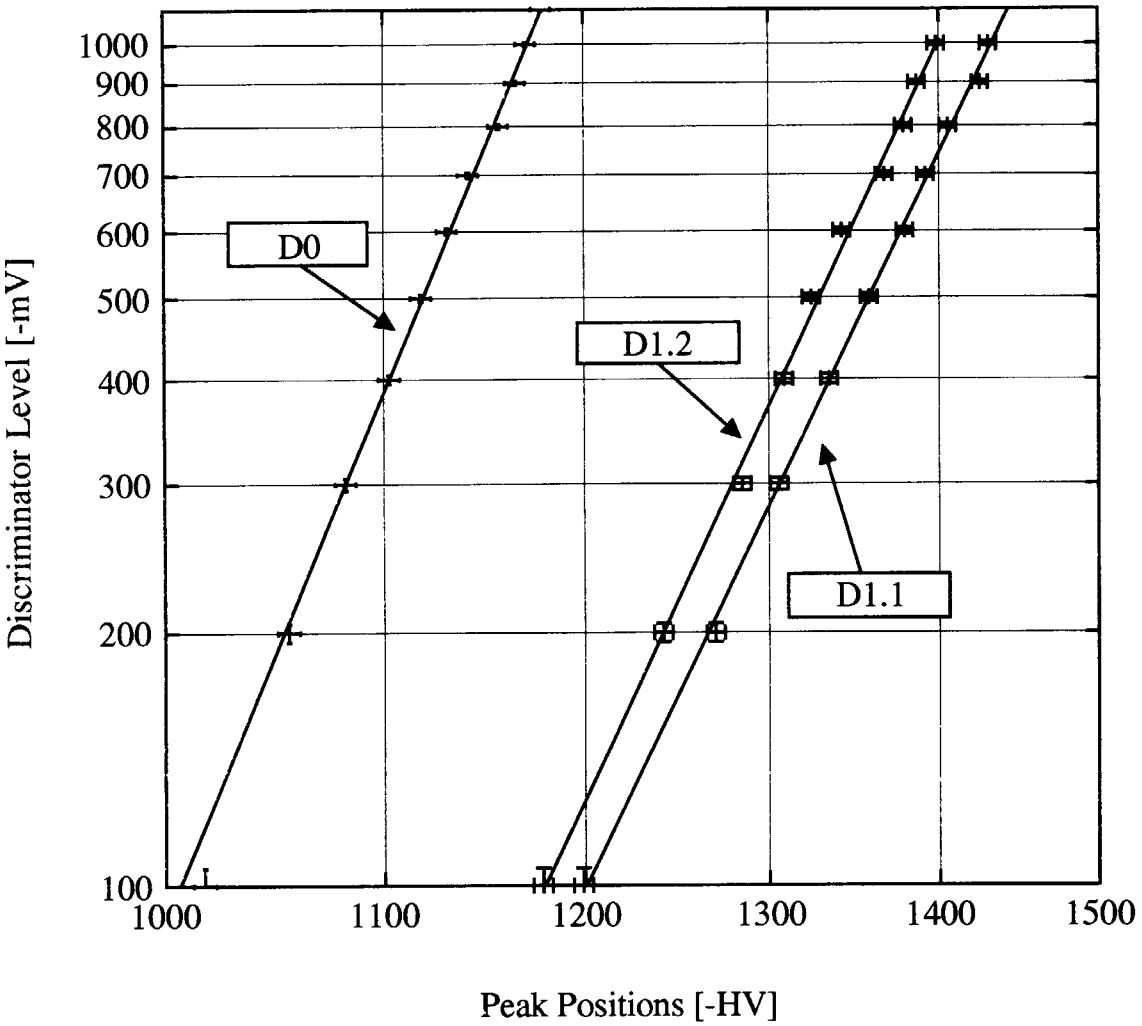

Figure 5. Results from the calibrations of the D0-, D1.1- and D1.2-detectors. The calibration parameters are obtained from a powerfit of the data. The slope (n_i) should be a number proportional to the number of dynodes of the PM-tube and is therefore approximately the same for all three detectors. The different values of the intercepts (K_{0i}) indicate the different sensitivities of the detectors.

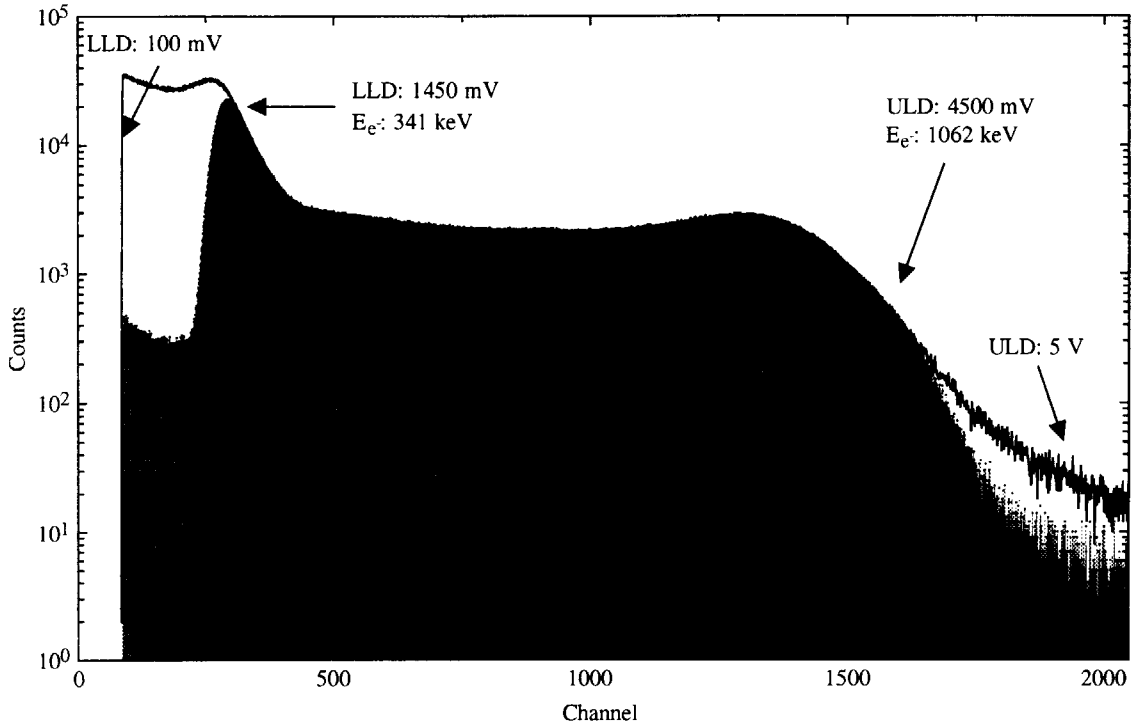

Figure 6. Test of the HV calibration of the D0 detector. The HV was set to 1200 V and the LLD- and the ULD-levels were set to the electron energies corresponding to the Compton edge energies of Na-22. As a reference, the pulse height spectrum with a maximum amplitude window is also shown.

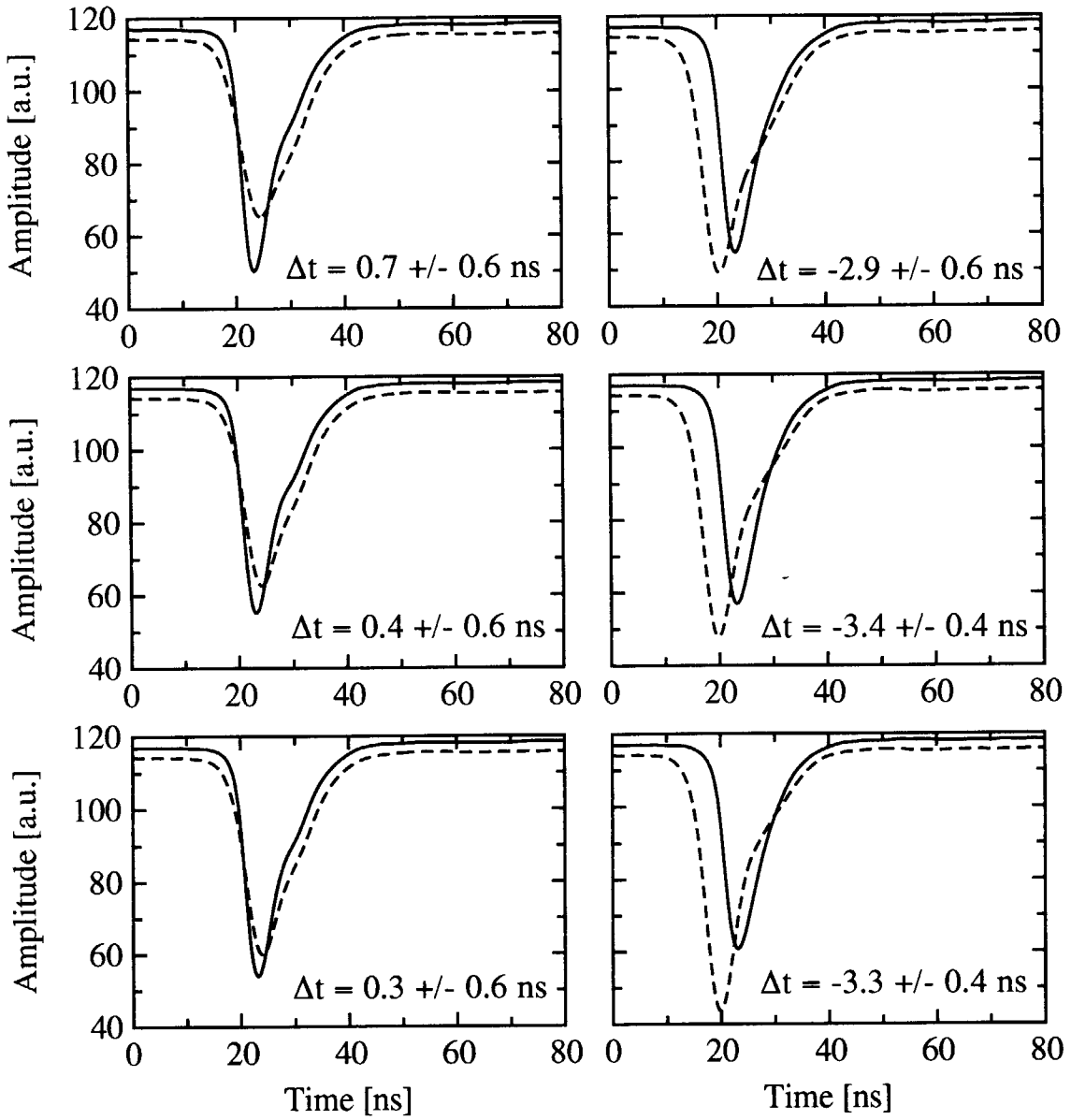

Figure 7. Averaged pulse shape from 1000 events. The left plots corresponds to a source position in the middle (vertical) of the D1 scintillator while the right plots correspond to source positions to the right (vertical) close to the D1.2 detector. The pulses from the D1.1- and the D1.2 detector are plotted with solid and hatched lines, respectively. The time difference between the pulses is calculated by correlation using the fast-Fourier transform.

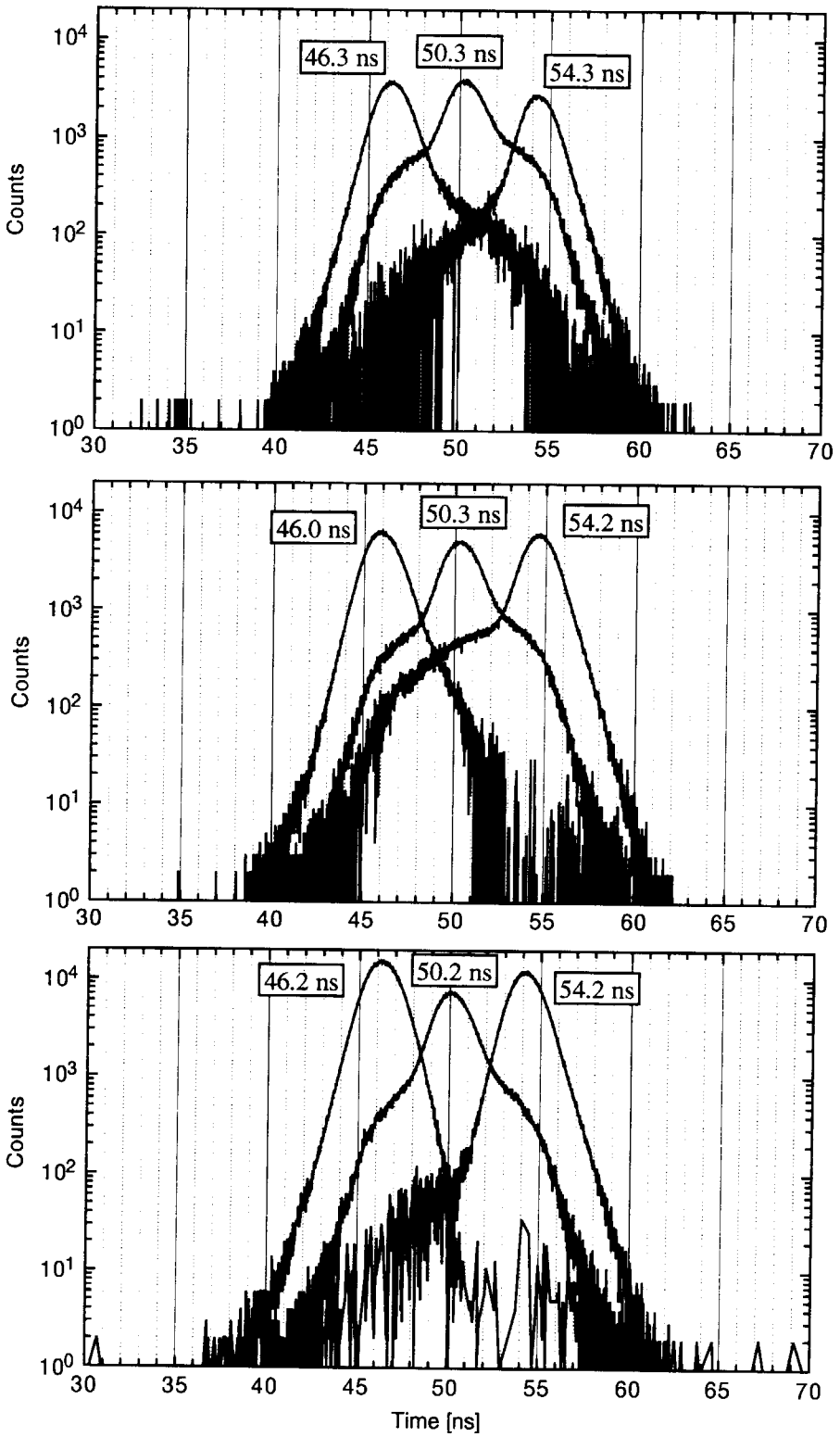

Figure 8. Time difference between the D1.1- and the D1.2 detectors, obtained from a TAC measurement. The D1.1 anode signal was delayed ~50 ns.

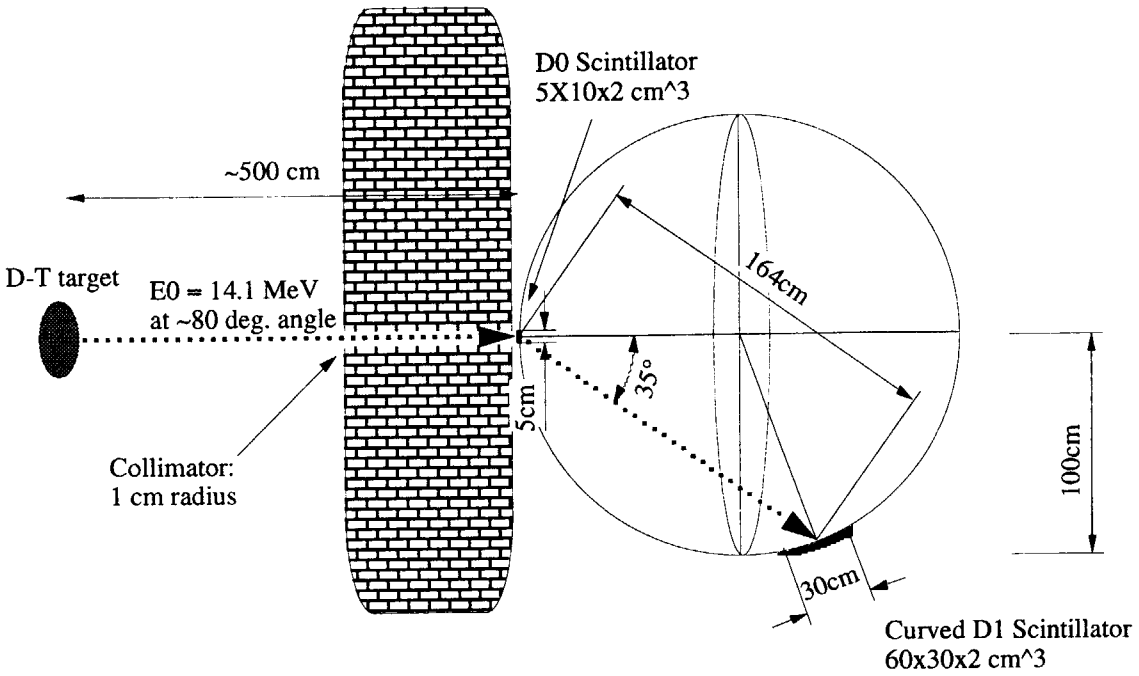

Figure 9. Setup of the t-o-f measurement at FNS. The DT target emits neutrons at an angle of ~80° with the beam-line. The collimated neutrons enter the D0 detector at a distance of ~500 cm from the target. Due to the small size of the collimator, the difference of the energy resolution between a tilted and a non-tilted D0 detector is marginal.

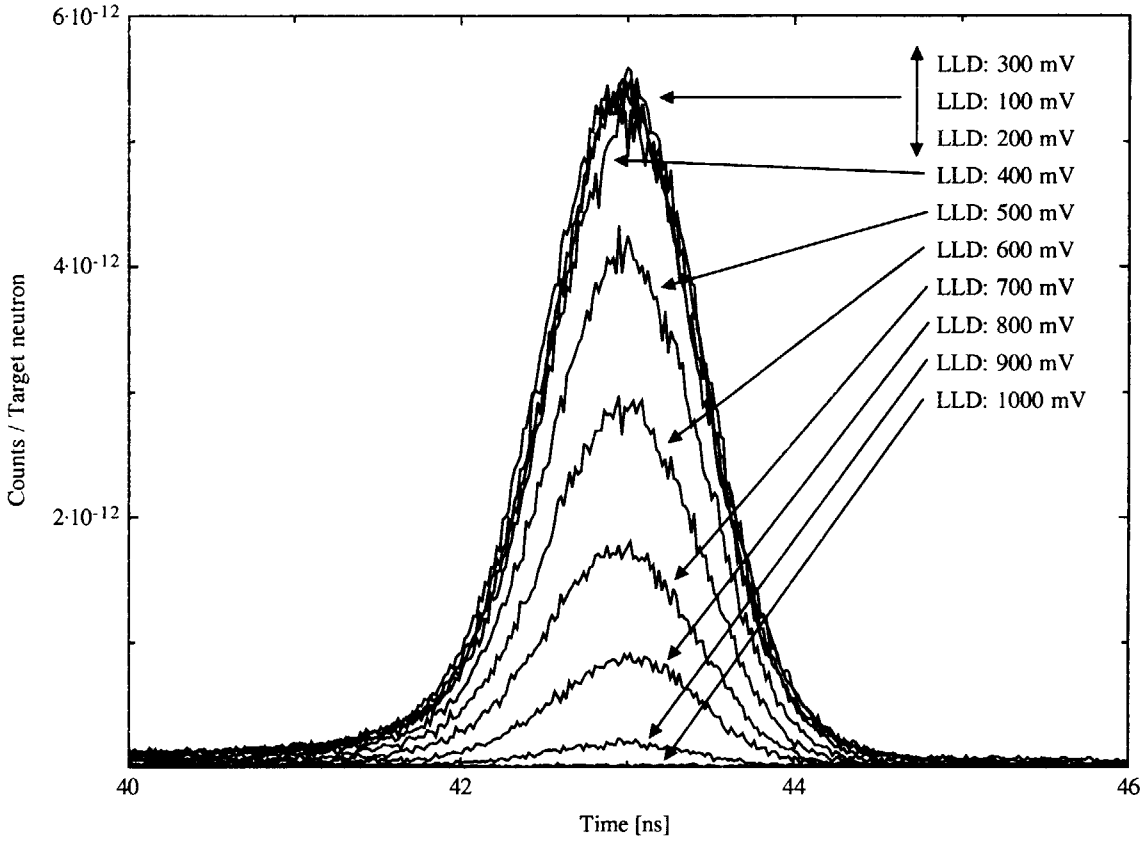

Figure 10. Neutron time distribution for coincidences from 14 MeV neutrons. The D0 LLD was scanned from 100 - 1000 mV. The proton energy range in the D0 detectors corresponds to 440 mV to 1000 mV.

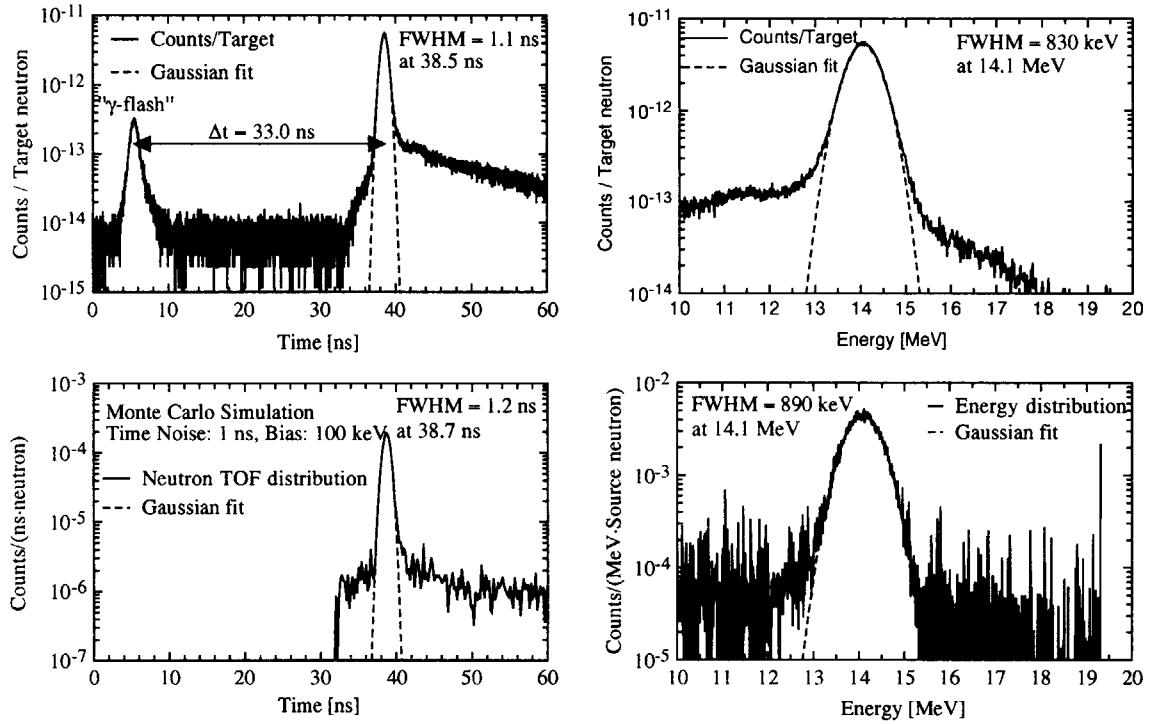

Figure 11. Comparison between a measured spectrum (upper graphs) and a Monte Carlo simulation (lower graphs). The measured spectrum was obtained from a test measurement utilizing 14 MeV source neutrons from the FNS neutron generator. The measured efficiency agreed within 15% and the measured resolution agreed within 6% compared with the calculated ones.

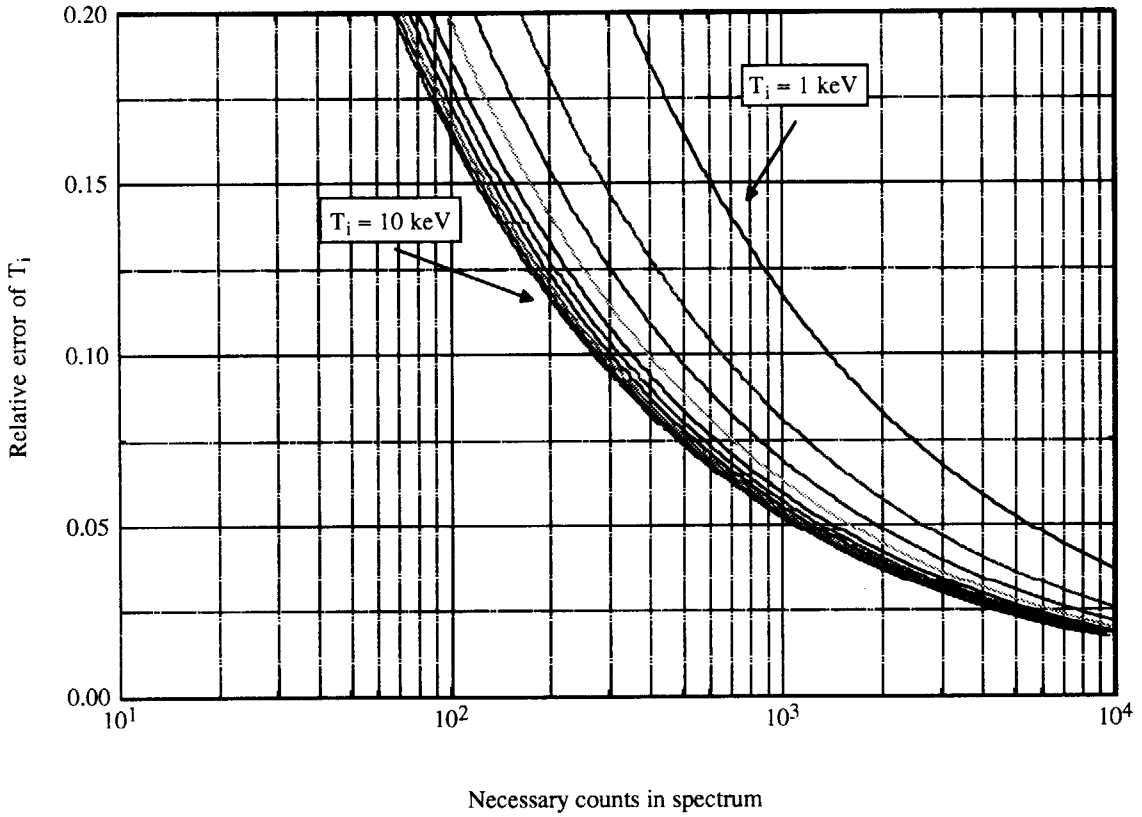

Figure 12. Relative error of the measurement of the ion temperature, T_i, vs. the number of integrated counts of a neutron energy distribution.

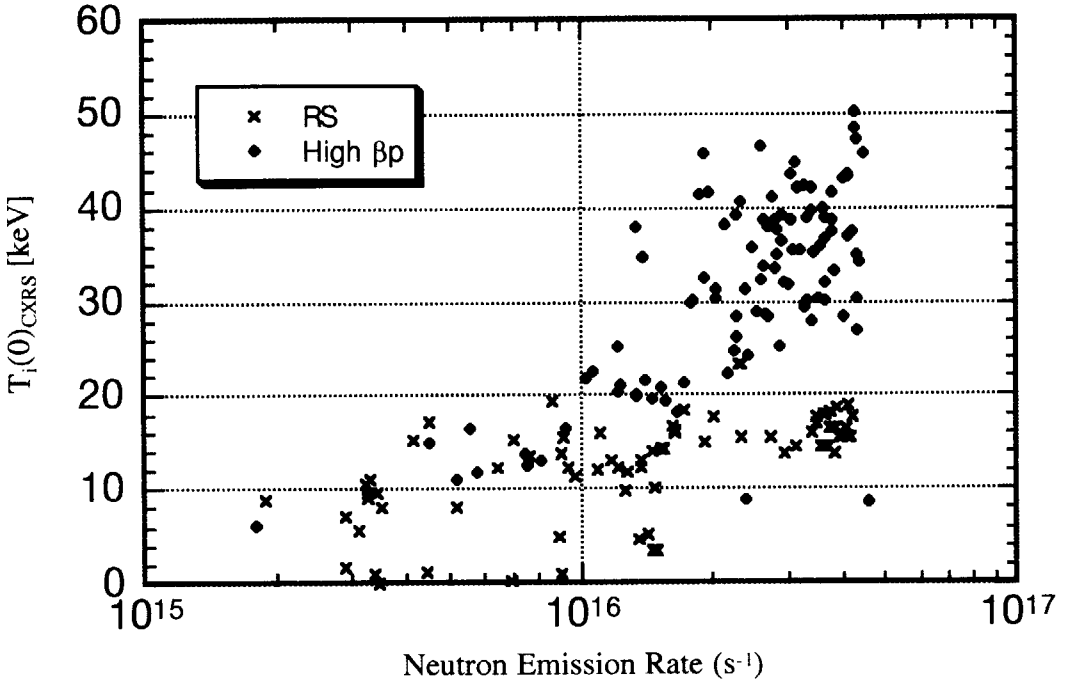

Figure 13. Ion temperature in the center of the plasma vs. the neutron emission rate. Two scenarios are shown, high β-poloidal and Reversed Shear plasmas.

国際単位系 (SI) と換算表

表 1　SI基本単位および補助単位

量	名　称	記　号
長　さ	メートル	m
質　量	キログラム	kg
時　間	秒	s
電　流	アンペア	A
熱力学温度	ケルビン	K
物質量	モル	mol
光　度	カンデラ	cd
平面角	ラジアン	rad
立体角	ステラジアン	sr

表 2　SIと併用される単位

名　称	記　号
分，時，日	min，h，d
度，分，秒	°，′，″
リットル	l，L
トン	t
電子ボルト	eV
原子質量単位	u

1 eV = 1.60218 × 10^{-19} J

1 u = 1.66054 × 10^{-27} kg

表 5　SI接頭語

倍数	接頭語	記　号
10^{18}	エクサ	E
10^{15}	ペタ	P
10^{12}	テラ	T
10^{9}	ギガ	G
10^{6}	メガ	M
10^{3}	キロ	k
10^{2}	ヘクト	h
10^{1}	デカ	da
10^{-1}	デシ	d
10^{-2}	センチ	c
10^{-3}	ミリ	m
10^{-6}	マイクロ	μ
10^{-9}	ナノ	n
10^{-12}	ピコ	p
10^{-15}	フェムト	f
10^{-18}	アト	a

表 3　固有の名称をもつSI組立単位

量	名　称	記号	他のSI単位による表現
周波数	ヘルツ	Hz	s^{-1}
力	ニュートン	N	m·kg/s^2
圧力，応力	パスカル	Pa	N/m^2
エネルギー，仕事，熱量	ジュール	J	N·m
工率，放射束	ワット	W	J/s
電気量，電荷	クーロン	C	A·s
電位，電圧，起電力	ボルト	V	W/A
静電容量	ファラド	F	C/V
電気抵抗	オーム	Ω	V/A
コンダクタンス	ジーメンス	S	A/V
磁束	ウェーバ	Wb	V·s
磁束密度	テスラ	T	Wb/m^2
インダクタンス	ヘンリー	H	Wb/A
セルシウス温度	セルシウス度	℃	
光束	ルーメン	lm	cd·sr
照度	ルクス	lx	lm/m^2
放射能	ベクレル	Bq	s^{-1}
吸収線量	グレイ	Gy	J/kg
線量当量	シーベルト	Sv	J/kg

表 4　SIと共に暫定的に維持される単位

名　称	記　号
オングストローム	Å
バーン	b
バール	bar
ガル	Gal
キュリー	Ci
レントゲン	R
ラド	rad
レム	rem

1 Å = 0.1 nm = 10^{-10} m

1 b = 100 fm^2 = 10^{-28} m^2

1 bar = 0.1 MPa = 10^5 Pa

1 Gal = 1 cm/s^2 = 10^{-2} m/s^2

1 Ci = 3.7 × 10^{10} Bq

1 R = 2.58 × 10^{-4} C/kg

1 rad = 1 cGy = 10^{-2} Gy

1 rem = 1 cSv = 10^{-2} Sv

（注）

1. 表1－5は「国際単位系」第5版，国際度量衡局 1985年刊行による。ただし，1 eVおよび1 uの値はCODATAの1986年推奨値によった。
2. 表4には海里，ノット，アール，ヘクタールも含まれているが日常の単位なのでここでは省略した。
3. barは，JISでは流体の圧力を表わす場合に限り表2のカテゴリーに分類されている。
4. EC閣僚理事会指令ではbar，barnおよび「血圧の単位」mmHgを表2のカテゴリーに入れている。

換　算　表

力

N(=10^5dyn)	kgf	lbf
1	0.101972	0.224809
9.80665	1	2.20462
4.44822	0.453592	1

粘　度　1 Pa·s(N·s/m^2) = 10 P(ポアズ)(g/(cm·s))

動粘度　1 m^2/s = 10^4 St(ストークス)(cm^2/s)

圧力

MPa(=10 bar)	kgf/cm^2	atm	mmHg(Torr)	lbf/in^2(psi)
1	10.1972	9.86923	7.50062 × 10^3	145.038
0.0980665	1	0.967841	735.559	14.2233
0.101325	1.03323	1	760	14.6959
1.33322 × 10^{-4}	1.35951 × 10^{-3}	1.31579 × 10^{-3}	1	1.93368 × 10^{-2}
6.89476 × 10^{-3}	7.03070 × 10^{-2}	6.80460 × 10^{-2}	51.7149	1

エネルギー・仕事・熱量

J(=10^7erg)	kgf·m	kW·h	cal(計量法)	Btu	ft·lbf	eV
1	0.101972	2.77778 × 10^{-7}	0.238889	9.47813 × 10^{-4}	0.737562	6.24150 × 10^{18}
9.80665	1	2.72407 × 10^{-6}	2.34270	9.29487 × 10^{-3}	7.23301	6.12082 × 10^{19}
3.6 × 10^6	3.67098 × 10^5	1	8.59999 × 10^5	3412.13	2.65522 × 10^6	2.24694 × 10^{25}
4.18605	0.426858	1.16279 × 10^{-6}	1	3.96759 × 10^{-3}	3.08747	2.61272 × 10^{19}
1055.06	107.586	2.93072 × 10^{-4}	252.042	1	778.172	6.58515 × 10^{21}
1.35582	0.138255	3.76616 × 10^{-7}	0.323890	1.28506 × 10^{-3}	1	8.46233 × 10^{18}
1.60218 × 10^{-19}	1.63377 × 10^{-20}	4.45050 × 10^{-26}	3.82743 × 10^{-20}	1.51857 × 10^{-22}	1.18171 × 10^{-19}	1

1 cal = 4.18605 J（計量法）

= 4.184 J　（熱化学）

= 4.1855 J　（15 °C）

= 4.1868 J（国際蒸気表）

仕事率　1 PS（仏馬力）

= 75 kgf·m/s

= 735.499 W

放射能

Bq	Ci
1	2.70270 × 10^{-11}
3.7 × 10^{10}	1

吸収線量

Gy	rad
1	100
0.01	1

照射線量

C/kg	R
1	3876
2.58 × 10^{-4}	1

線量当量

Sv	rem
1	100
0.01	1

（86年12月26日現在）

THE JT-60U 2.45 MeV NEUTRON TIME-OF-FLIGHT SPECTROMETER